Modeling of the intrinsic stress effect on the resonant frequency of NEMS resonators integrated by beams with…

Article *in* Microsystem Technologies · December 2010

DOI: 10.1007/s00542-010-1134-5

5 authors, including:

Agustin Leobardo Herrera-May
Universidad Veracruzana
66 PUBLICATIONS **353** CITATIONS
SEE PROFILE

Luz A Aguilera-Cortés
Universidad de Guanajuato
58 PUBLICATIONS **285** CITATIONS
SEE PROFILE

Miguel Torres-Cisneros
Universidad de Guanajuato
202 PUBLICATIONS **424** CITATIONS
SEE PROFILE

Microsyst Technol (2010) 16:2067–2074
DOI 10.1007/s00542-010-1134-5

TECHNICAL PAPER

Modeling of the intrinsic stress effect on the resonant frequency of NEMS resonators integrated by beams with variable cross-section

A. L. Herrera-May · L. A. Aguilera-Cortés · P. J. García-Ramírez · H. Plascencia-Mora · M. Torres-Cisneros

Received: 20 April 2010 / Accepted: 18 August 2010 / Published online: 2 September 2010

Abstract Nano-electro-mechanical systems (NEMS) resonators integrated by a double clamped beam with variable cross-section are used in several applications such as chemical and biological detectors, high-frequency filters, and signal processing. The structure of these resonators can experience intrinsic stresses produced during their fabrication process. We present an analytical model to estimate the first bending resonant frequency of NEMS resonators based on a double clamped beam with three cross-sections, which considers the intrinsic stress effect on the resonant structure. This model is obtained using the Rayleigh and Macaulay methods, as well as the Euler–Bernoulli beam theory. We applied the analytical model to a silicon carbide (SiC) resonator of 186 nm thickness reported in the literature. This resonator has a total length ranking from 80 to 258 μm and is subjected to a tensile intrinsic stress close to 110 MPa. Results from this model show good agreement with experimental results. The analytic frequencies have a maximum relative difference less than 6.3% respect to the measured frequencies. The tensile intrinsic stress on the resonant structure causes a significantly increase on its bending resonant frequency. The proposed model provides an insight into the study of the intrinsic stress influence on the resonant frequency of this nanostructure. In addition, this model can estimate the frequency shift due to the variations of the resonator geometrical parameters.

A. L. Herrera-May (✉) · P. J. García-Ramírez
Centro de Investigación en Micro y Nanotecnología, Universidad Veracruzana, 94292 Boca del Río, Veracruz, Mexico
e-mail: leherrera@uv.mx

A. L. Herrera-May · L. A. Aguilera-Cortés · H. Plascencia-Mora · M. Torres-Cisneros
Depto. Ingeniería Mecánica, Campus Irapuato-Salamanca, Universidad de Guanajuato, Carretera Salamanca-Valle de Santiago km 3.5 + 1.8 km, Salamanca, Guanajuato, Mexico

L. A. Aguilera-Cortés
e-mail: aguilera@salamanca.ugto.mx

M. Torres-Cisneros
MQW Group, CREOL, University of Central Florida, Orlando, FL 32826, USA
e-mail: mtorresc@creol.ucf.edu

1 Introduction

Nano-electro-mechanical systems (NEMS) resonators present important attributes such as miniscule mass, small size, high resonant frequency, low operating power, and high quality factor (Ekinci and Roukes 2005; Herrera-May et al. 2010). Due to this, NEMS resonators offer great promise for a wide range of applications, including mechanical signal processing (Baldwin et al. 2006), mass and biological sensing (Waggoner et al. 2009; Varshney et al. 2009), electro-thermal tunability (Jun et al. 2006; Jun et al. 2008), force detection (Mamin and Rugar 2001), ultra-high frequency oscillators (Feng et al. 2008), switching (Guerra et al. 2008), parametric amplifiers (Karabalin et al. 2009), and study of oscillatory fluid dynamics (Karabacak et al. 2007).

The mechanical design of several NEMS resonators is based on a double clamped beam with constant cross-section. However, part of the two fixed supports of this beam can be etched during its release process, producing a double clamped beam with variable cross-section. Thus, resonant beam presents three cross-sections with the same

thickness, but with different width and length, respectively. Normally, this beam is excited on its fundamental bending or torsional mode. For this case, the study of the resonant frequency and mechanical behavior of a double clamped beam must consider the effect of its undercut supports. This resonator type is commonly used in mass and biological detectors (Naik et al. 2009; Cleland et al. 2001). The intrinsic stress/strain on the resonant structure changes its mechanical performance and resonant frequency. Thus, intrinsic stress on NEMS resonators can be used to improve their performance (Cimalla et al. 2007). This intrinsic stress/strain is caused by the lattice mismatch as well as differences in thermal expansion coefficient among epitaxial layers and substrate (Cimalla et al. 2007). Cimalla et al. 2006 developed NEMS resonators based on double clamped beams of aluminum nitride (AlN) and silicon carbide (SiC), which registered an increase in their bending resonant frequencies and quality factors at atmospheric pressure due to the tensile intrinsic stress on the resonators. The intrinsic stress effect on NEMS resonators should be considered to determine their fundamental resonant frequencies.

Bouwstra and Geijselaers (1991) presented a one-dimensional model that includes the axial force effect on the bending resonant frequency of a double clamped beam with a constant cross-section. The axial force on the beam is caused by an intrinsic stress inside it. In this model, a tension axial force increases the bending resonant frequency of the beam; however, a compressive axial force decreases its frequency. Ikehara et al. (2001) developed an analytical model to calculate the bending resonant frequency of a doubly supported beam under the influence of an intrinsic strain, but this model only considers beams with a constant cross-section. Rao (2004) reported an analytical solution to obtain the bending resonant frequency of simply supported and double clamped beams subject to an axial force; although, this solution is also limited to beams with constant cross-section. Other researches (Galef 1968; Bokaian 1988) have found analytical solutions to determine the bending resonant frequency of beams with uniform cross-section, different end conditions and subject to axial loads. Nevertheless, these analytical models do not consider changes in the beam cross-section. Lobontiu (2006, 2007) built interesting analytical models to calculate the resonant frequency of doubly clamped beams with variable cross-sections, but without including the intrinsic stress effect. In order to overcome this problem, we propose an analytical model to estimate the bending resonant frequency of NEMS resonators integrated by double clamped beams with three cross-sections, which are subjected to intrinsic stress. This model is based on the Macaulay and Rayleigh methods, as well as the Euler–Bernoulli beam theory.

After this introduction, the paper is organized as follows. Section 2 presents the description of the analytic model considering a double clamped beam subject to intrinsic stress, which has a variable cross-section. Section 3 shows the analytic model results considering a SiC resonator reported in the literature. In addition, a finite element method (FEM) model of this resonator using the ANSYS® software is presented. The paper ends with the concluding discussion and a proposal for further work.

2 Description of the analytical model

In this section, we present the description of the analytical model proposed in this work, which is obtained through the Macaulay and Rayleigh methods, as well as Euler–Bernoulli beam theory.

Figure 1 shows a NEMS resonator formed by a double clamped beam with three cross-sections. This structural configuration is obtained after a release process of the main beam, where the supporting substrate is isotropically etched and the beam supports are undercut. In this work, we consider the influence of both etching supports and the intrinsic stress effect on the bending resonant frequency of the beam. This intrinsic stress is produced during the beam's release process. Figure 2 depicts the geometrical parameters of NEMS resonator, where both beam supports have the same length ($L_1 = L_3$). The weight per unit length in each section of the beam is represented by uniformly distributed loads. Figure 3 shows the reaction loads and bending moments at the beam clamping points.

The Rayleigh method establishes the lowest bending resonant frequency (f_{res}) of a resonator under a mass and stiffness distribution variation (Rao 2004). It estimates the natural frequency assuming energy conservation in the resonant structure; thus, the maximum kinetic energy (T_m)

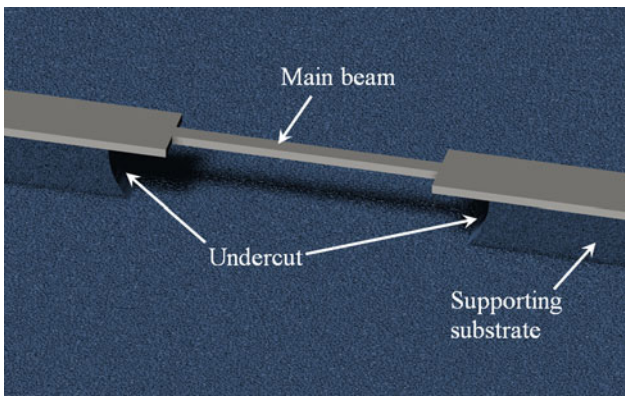

Fig. 1 A 3D schematic view of a NEMS resonator integrated by a double clamped beam with three cross-sections

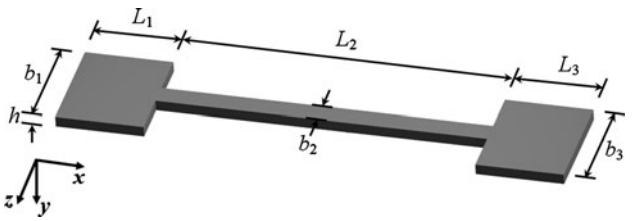

Fig. 2 Schematic view of the geometrical parameters of a double clamped beam with three cross-sections

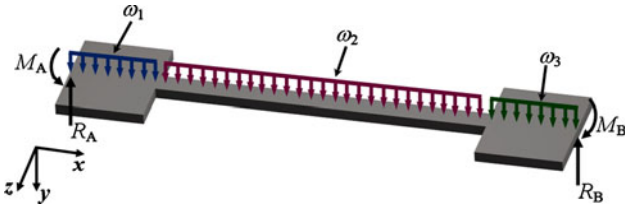

Fig. 3 Reaction loads, bending moments, and weight per unit length on the double clamped beam with three cross-sections

is equal to the maximum potential energy (U_m) (Weaver et al. 1990):

$$T_m = U_m. \tag{1}$$

We regard a harmonic motion of the resonator whose bending deflection at a given point of its structure is obtained as a product between a spatial function $y(x)$ and a time-dependent one (Rao 2004; Lobontiu 2007):

$$y(x,t) = y(x)\sin(2\pi ft), \tag{2}$$

where t is the time and f is the frequency.

Besides, we consider a tensional intrinsic stress (σ) inside of the beam, which generates a tensional axial load (P) on it. For the case of a compressive intrinsic stress on the resonator, the sign of this axial load will be negative. The intrinsic stress is produced during the beam's release process. For the case of out-of plane bending, the maximum potential (U_m) and kinetic (T_m) energies of the double clamped beam with three cross-sections are given by (Weaver et al. 1990; Virgin 2007):

$$\begin{aligned} U_m = {} & \frac{EI_1}{2}\int_0^{L_1}\left(\frac{\partial^2 y_1(x)}{\partial x^2}\right)^2 dx + \frac{P}{2}\int_0^{L_1}\left(\frac{\partial y_1(x)}{\partial x}\right)^2 dx \\ & + \frac{EI_2}{2}\int_{L_1}^{L_{12}}\left(\frac{\partial^2 y_2(x)}{\partial x^2}\right)^2 dx + \frac{P}{2}\int_{L_1}^{L_{12}}\left(\frac{\partial y_2(x)}{\partial x}\right)^2 dx \\ & + \frac{1}{2}EI_3\int_{L_{12}}^{L_{123}}\left(\frac{\partial^2 y_3(x)}{\partial x^2}\right)^2 dx + \frac{P}{2}\int_{L_{12}}^{L_{123}}\left(\frac{\partial y_3(x)}{\partial x}\right)^2 dx, \end{aligned} \tag{3}$$

$$\begin{aligned} T_m = \vartheta^2 \Bigg[& \frac{\rho b_1 h_1}{2}\int_0^{L_1}(y_1(x))^2 dx + \frac{\rho b_2 h_2}{2}\int_{L_1}^{L_{12}}(y_2(x))^2 dx \\ & + \frac{\rho b_3 h_3}{2}\int_{L_{12}}^{L_{123}}(y_3(x))^2 dx \Bigg], \end{aligned} \tag{4}$$

where $\vartheta = 2\pi f$, $L_{12} = L_1 + L_2$, $L_{123} = L_1 + L_2 + L_3$, $y_j(x)$, b_j, h_j and I_j are the bending deflection, width, thickness and moment of inertia in the jth beam section, as well E and ρ are the elastic modulus and density of beam, respectively.

Substituting Eqs. 3 and 4 into Eq. 1, the lowest bending resonant frequency (f_r) for a double clamped beam is determined by

$$f_r = \frac{1}{2\pi}\left(\frac{U_m}{T_m/\vartheta^2}\right)^{1/2}. \tag{5}$$

The bending deflection $y_j(x)$ in each section of the beam can be obtained through the Euler–Bernoulli beam theory (Rao 2004) and the Macaulay method (Craig 1996). We assume small deflections and isotropic material on the resonant structure; therefore, the bending deflections are calculated from:

$$EI_1\frac{\partial^2 y_1(x)}{\partial x^2} = M_1(x),\ 0<x<L_1, \tag{6a}$$

$$EI_2\frac{\partial^2 y_2(x)}{\partial x^2} = M_2(x),\ L_1<x<L_{12}, \tag{6b}$$

$$EI_3\frac{\partial^2 y_3(x)}{\partial x^2} = M_3(x),\ L_{12}<x<L_{123}, \tag{6c}$$

where $M_j(x)$ is the bending moment in the jth beam section and it is represented by Macaulay functions.

The bending deflections in each section of the beam must fulfill the following conditions:

$$\begin{aligned} & y_1(0) = 0, && \frac{\partial y_1(0)}{\partial x} = 0, \\ & y_1(L_1) = y_2(L_1), && \frac{\partial y_1(L_1)}{\partial x} = \frac{\partial y_2(L_1)}{\partial x}, \\ & y_2(L_{12}) = y_3(L_{12}), && \frac{\partial y_2(L_{12})}{\partial x} = \frac{\partial y_3(L_{12})}{\partial x}, \end{aligned} \tag{7}$$

The Macaulay method can represent several load types on beams with different cross-sections (Bolton 2006), through a bracket notation function $\langle x-a\rangle^n$ (Stephen 2007), which have a zero value for $x < a$ as well as $(x-a)^n$ for $x \geq a$. The n exponent accepts three values: $n = 0$ for a uniformly distributed load, $n = -1$ for a concentrated load, and $n = -2$ for a bending moment on the beam (Craig 1996), respectively.

The load function $q(x)$ of the resonator is obtained using the Macaulay functions:

$$q(x) = -M_A\langle x-0\rangle^{-2} + R_A\langle x-0\rangle^{-1} - \omega_1\langle x-0\rangle^{0} + \omega_1\langle x-L_1\rangle^{0} - \omega_2\langle x-L_1\rangle^{0} + \omega_2\langle x-L_{12}\rangle^{0} - \omega_3\langle x-L_{12}\rangle^{0} + \omega_3\langle x-L_{123}\rangle^{0} + R_B\langle x-L_{123}\rangle^{-1} + M_B\langle x-L_{123}\rangle^{-2}. \quad (8)$$

Based on the integration rules of the Macaulay functions (Craig 1996), the shear load function $V(x)$ acting on the beam cross-sections is obtained integrating Eq. 8 with respect to x:

$$V(x) = -M_A\langle x-0\rangle^{-1} + R_A\langle x-0\rangle^{0} - \omega_1\langle x-0\rangle^{1} + \omega_1\langle x-L_1\rangle^{1} - \omega_2\langle x-L_1\rangle^{1} + \omega_2\langle x-L_{12}\rangle^{1} - \omega_3\langle x-L_{12}\rangle^{1} + \omega_3\langle x-L_{123}\rangle^{1} + R_B\langle x-L_{123}\rangle^{0} + M_B\langle x-L_{123}\rangle^{-1} + C_1. \quad (9)$$

The bending moment function $M(x)$ on the beam is determined integrating $V(x)$ with respect to x:

$$M(x) = -M_A\langle x-0\rangle^{0} + R_A\langle x-0\rangle^{1} - \frac{1}{2}\omega_1\langle x-0\rangle^{2} + \frac{1}{2}\omega_1\langle x-L_1\rangle^{2} - \frac{1}{2}\omega_2\langle x-L_1\rangle^{2} + \frac{1}{2}\omega_2\langle x-L_{12}\rangle^{2} - \frac{1}{2}\omega_3\langle x-L_{12}\rangle^{2} + \frac{1}{2}\omega_3\langle x-L_{123}\rangle^{2} + R_B\langle x-L_{123}\rangle^{1} + M_B\langle x-L_{123}\rangle^{0} + C_1x + C_2, \quad (10)$$

where C_1 and C_2 are constants calculated through the boundary conditions of the shear and moment functions.

Assuming the same length and width on the first and third section of the beam; then, we found that the reaction loads and bending moments satisfy the following conditions: $R_A = R_B$ and $M_A = M_B$. The boundary conditions of the shear and moment functions at the beam clamping ends are: $V(0) = R_A$ and $M(0) = M_A$. Using these conditions in Eqs. 9 and 10, we calculated $C_1 = C_2 = 0$.

Due to the symmetry of the double clamped beam, the weights per unit length of the first and third section are equal ($\omega_1 = \omega_3$). These weights are determined as:

$$\omega_j = \rho g b_j h_j, \quad (11)$$

where g is the gravitational acceleration.

Regarding $\omega_1 = \omega_3$, the reaction loads ($R_A = R_B$) and bending moments ($M_A = M_B$) on the both beam ends are expressed as:

$$R_A = \frac{1}{2}(2\omega_1 L_1 + \omega_2 L_2), \quad (12)$$

$$M_A = \left(2L_1 + \frac{I_3}{I_2}L_2\right)^{-1} \times \left\{\frac{I_3}{I_2}\left[\frac{1}{2}R_A L_2(2L_1+L_2) - \frac{1}{2}\omega_1 L_1 L_2 L_{12} - \frac{1}{6}\omega_2 L_2^3\right] + R_A L_1(2L_1+L_2) - \frac{1}{3}\omega_1 L_1^2(4L_1+3L_2) - \frac{1}{2}\omega_2 L_1 L_2 L_{12}\right\}. \quad (13)$$

Using Eq. 10, we get the following bending moments in the three sections of the resonator. For $0 < x < L_1$:

$$M_1(x) = -M_A\langle x-0\rangle^{0} + R_A\langle x-0\rangle^{1} - \frac{1}{2}\omega_1\langle x-0\rangle^{2}. \quad (14)$$

For $L_1 < x < L_{12}$:

$$M_2(x) = -M_A\langle x-0\rangle^{0} + R_A\langle x-0\rangle^{1} - \frac{1}{2}\omega_1\langle x-0\rangle^{2} + \frac{1}{2}\omega_1\langle x-L_1\rangle^{2} - \frac{1}{2}\omega_2\langle x-L_1\rangle^{2}. \quad (15)$$

For $L_{12} < x < L_{123}$:

$$M_3(x) = -M_A\langle x-0\rangle^{0} + R_A\langle x-0\rangle^{1} - \frac{1}{2}\omega_1\langle x-0\rangle^{2} + \frac{1}{2}\omega_1\langle x-L_1\rangle^{2} - \frac{1}{2}\omega_2\langle x-L_1\rangle^{2} + \frac{1}{2}\omega_2\langle x-L_{12}\rangle^{2} - \frac{1}{2}\omega_3\langle x-L_{12}\rangle^{2}. \quad (16)$$

These bending moment equations are substituted in Eq. 6a–6c; after, it is integrated twice respect to x in order to obtain the bending deflection in each beam section. For this, we use the integration rules of the Macaulay functions (Craig 1996) and the boundary conditions indicated by Eq. 7. Thus, the bending deflections are given by: For $0 < x < L_1$:

$$y_1(x) = \frac{1}{EI_1}\left[-\frac{1}{2}M_A\langle x-0\rangle^{2} + \frac{1}{6}R_A\langle x-0\rangle^{3} - \frac{1}{24}\omega_1\langle x-0\rangle^{4}\right]. \quad (17)$$

For $L_1 < x < L_{12}$:

$$y_2(x) = \frac{1}{EI_2}\left[-\frac{1}{2}M_A\langle x-0\rangle^{2} + \frac{1}{6}R_0\langle x-0\rangle^{3} - \frac{1}{24}\omega_1\langle x-0\rangle^{4} + \frac{1}{24}\omega_1\langle x-L_1\rangle^{4} - \frac{1}{24}\omega_2\langle x-L_1\rangle^{4} - \frac{1}{2}M_A L_1^2 + \frac{1}{3}R_A L_1^3 - \frac{1}{8}\omega_1 L_1^4 + \left(M_A L_1 - \frac{1}{2}R_A L_1^2 + \frac{1}{6}\omega_1 L_1^3\right)x\right] + \frac{1}{EI_1}\left[\left(-M_A L_1 + \frac{1}{2}R_A L_1^2 - \frac{1}{6}\omega_1 L_1^3\right)x + \frac{1}{2}M_A L_1^2 - \frac{1}{3}R_A L_1^3 + \frac{1}{8}\omega_1 L_1^4\right]. \quad (18)$$

For $L_{12} < x < L_{123}$:

$$y_3(x) = \frac{1}{EI_3}\left[-\frac{1}{2}M_A\langle x-0\rangle^{2} + \frac{1}{6}R_A\langle x-0\rangle^{3} - \frac{1}{24}\omega_1\langle x-0\rangle^{4} + \frac{1}{24}\omega_1\langle x-L_1\rangle^{4} - \frac{1}{24}\omega_2\langle x-L_1\rangle^{4} + \frac{1}{24}\omega_2\langle x-L_{12}\rangle^{4} - \frac{1}{24}\omega_3\langle x-L_{12}\rangle^{4} + C_3x + C_4\right], \quad (19)$$

with

$$C_3 = \frac{I_3}{I_2}\left[-M_A L_2 + \frac{1}{2}R_A L_2(2L_1 + L_2) - \frac{1}{2}\omega_1 L_1 L_2 L_{12} - \frac{1}{6}\omega_2 L_2^3\right] + M_A L_2 - \frac{1}{2}R_A L_2(2L_1 + L_2) + \frac{1}{2}\omega_1 L_1 L_2 L_{12} + \frac{1}{6}\omega_2 L_2^3,$$

$$C_4 = \frac{I_3}{I_2}\left[\frac{1}{2}M_A L_2(2L_1 + L_2) - \frac{1}{3}R_A L_2(3L_1^2 + 3L_1 L_2 + L_2^2) + \frac{1}{12}\omega_1 L_1 L_2(6L_1^2 + 9L_1 L_2 + 4L_2^2) + \frac{1}{24}\omega_2 L_2^3(4L_1 + 3L_2)\right] - \frac{1}{2}M_A L_2(2L_1 + L_2) + \frac{1}{3}R_A L_2\left[3L_1(L_1 + L_2) + L_2^2\right] - \frac{1}{12}\omega_1 L_1 L_2\left[3L_1(2L_1 + 3L_2) + 4L_2^2\right] - \frac{1}{24}\omega_2 L_2^3(4L_1 + 3L_2).$$

After, we find the maximum potential and kinetic energies of the proposed resonator through the substitution of Eqs. 17–19 in Eqs. 3 and 4. Then, substituting these energies into Eq. 5, we determine the bending resonant frequency of the double clamped beam with three cross-sections.

Our analytical model will be compare with the experimental results reported by Cimalla et al. (2006) and the analytical model developed by Ikehara et al. (2001) that estimate the first bending resonant frequency (f_{rI}) of a double clamped beam with uniform cross-section and subjected to an internal strain (ε):

$$f_{rI} = 1.028\sqrt{\frac{E}{\rho}}\frac{h}{L^2}\sqrt{1 + 0.295\left(\frac{L}{h}\right)^2}\varepsilon, \tag{20}$$

where h is the thickness and L is length of the beam with uniform cross-section.

3 Results and discussions

In this section, we used the proposed model to determine the bending resonant frequency of a NEMS resonator based on a double clamped beam with three cross-sections, which is subjected to a tensile intrinsic stress.

Our analytical model is applied to a NEMS resonator fabricated by Cimalla et al. (2006) that is integrated by a double clamped beam with three cross-sections. This resonator has the same structural configuration respect to resonant beam shown in Fig. 1. Cimalla et al. (2006) fabricated the resonator using a SiC layer of 186 nm thickness on a silicon substrate. Table 1 shows the geometrical dimensions of this resonator; additionally, the material properties of the resonator used in the analytical model are: density of 3,210 kg/m^3 and elastic modulus of 424 GPa

Table 1 Dimensions of the geometrical parameters of the NEMS resonator

Geometrical parameter	Dimension (μm)
h	0.186
b_1, b_3	10.0
b_2	4.0
L_1, L_3	4.0
L_2	72–250

(Jackson et al. 2005). Due to the fabrication process, Cimalla et al. (2006) measured a tensile intrinsic strain (2.6×10^{-4}) on the beam employing X-ray diffraction and infrared ellipsometry. Based on this strain, we assumed a tensile intrinsic stress ($\sigma = E\varepsilon$) inside the beam close to 110 MPa. Thus, we obtained a tensile axial load (P) of 82 μN, considering the cross-section of the main beam. The strain and axial load were substituted into our analytic model and the analytical model reported by Ikehara et al. (2001) to find the first bending resonant frequency of the resonator designed by Cimalla et al. (2006). Regarding different beam total lengths (from 80 to 258 μm), the results of our analytic model agree very well with those experimentally measured by Cimalla et al. (2006), as shown in Fig. 4. Our analytic results have a relative difference less than 6.3% with respect to those measured by Cimalla. However, the analytical model's results

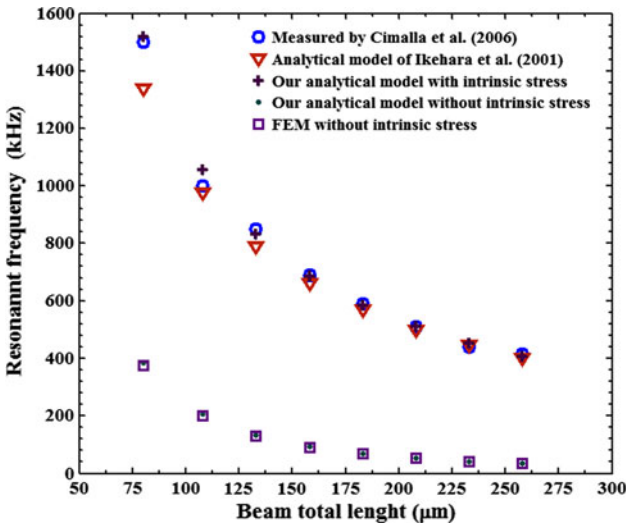

Fig. 4 Results of the first bending resonant frequency of a NEMS resonator developed by Cimalla et al. (2006) as a function of resonator total length. This resonator is under the influence of a tensile intrinsic stress. The resonant frequencies obtained through our analytic model presented a close relationship with the measured frequencies by Cimalla. Neglecting the intrinsic stress on the resonator, the resonant frequencies had a significantly decrease respect to the experimental ones. Experimental data reprinted with permission from Cimalla et al. (2006)

developed Ikehara et al. (2001) have a relative difference less than 10.8% with respect to the experimental results (see Fig. 4). Our analytical model presents better results

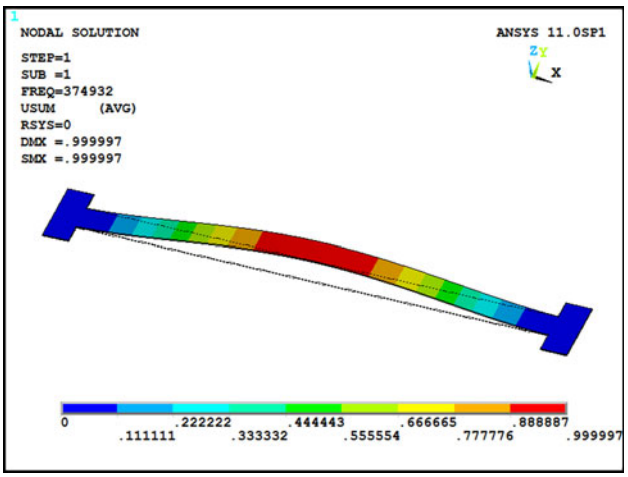

Fig. 5 First bending mode shape of the double clamped beam with three cross-sections

than those obtained by the analytical model reported by Ikehara et al. (2001). This is due to our model, which considers the influence of the undercut supports on the double clamped beam that originates a beam with three cross-sections. On the other hand, the model of Ikehara et al. (2001) is only employed for double clamped beams with constant cross-section. Nevertheless, the resonant frequencies obtained by both analytical models present a similar behavior to the measured frequencies when the beam total length increases. Thus, the resonant frequencies decrease inversely proportional with respect to the beam length.

Moreover, we found the resonant frequency of the resonator developed by Cimalla et al. (2006) without setting the intrinsic stress inside it. For this case, we substituted the load $P = 0$ in our analytic model. Also, we built a FEM model for the resonator through the ANSYS® software. The FEM model employs solid95 elements, which have three degrees of freedom per node (translations in the nodal x, y, and z directions). Neglecting the intrinsic stress on the resonator, the results of our analytic

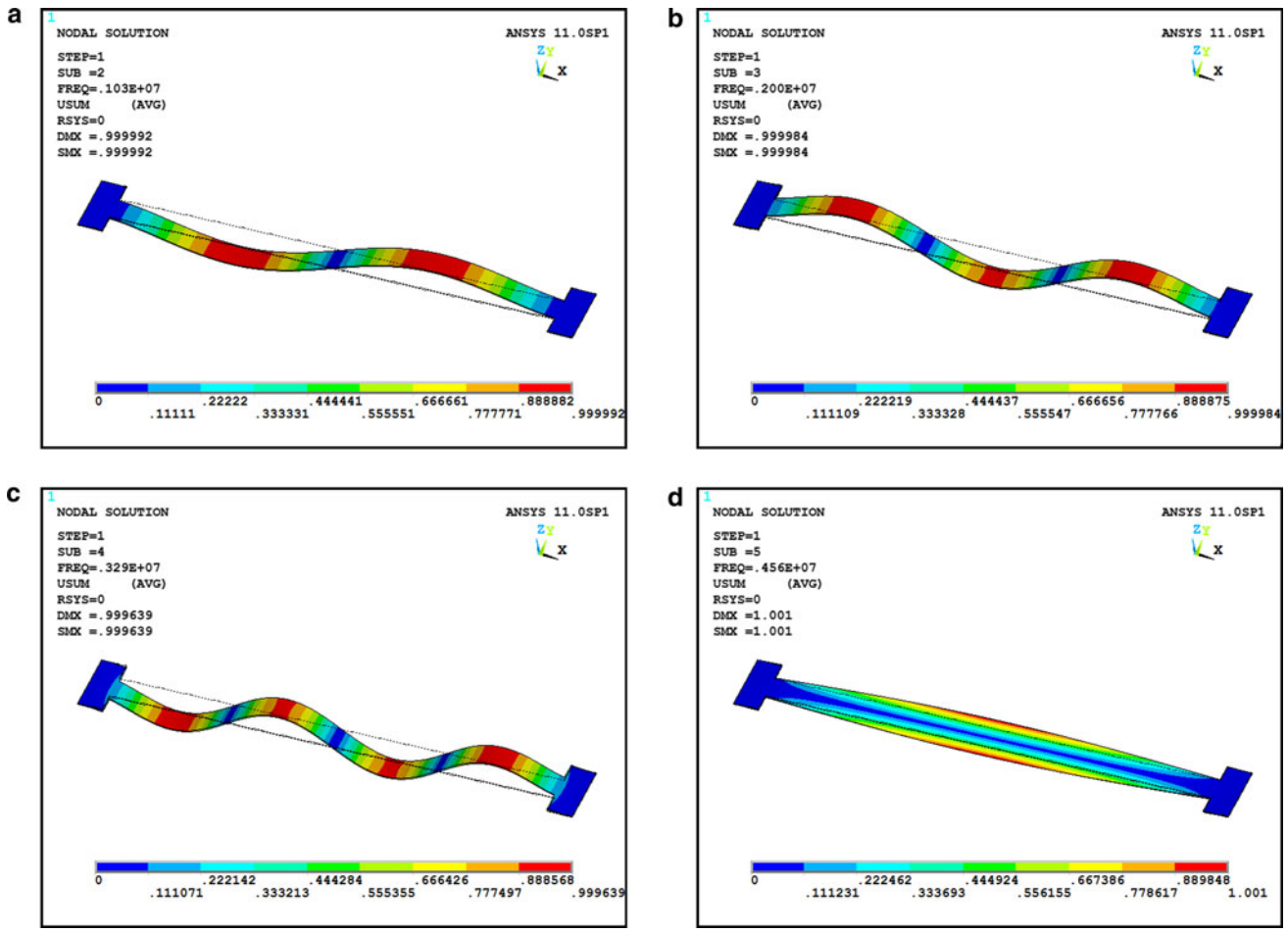

Fig. 6 **a** Second, **b** third, **c** fourth, and **d** fifth modal shapes of the double clamped beam with three cross-sections

and FEM models agree well, registering a relative difference less than 2.7% (see Fig. 4). However, these results showed a large difference respect to those that include the intrinsic stress on the resonator. Therefore, the tensile intrinsic stress significantly increased the first bending resonant frequency of the Cimalla's resonator. This is because of the increase in the maximum potential energy of the resonator. Figure 5 shows the first bending modal shape of the FEM model considering $L_2 = 72$ μm, which does not include the intrinsic stress. Figure 6 represents the following four modal shapes of this FEM model, where the fifth mode had a torsional shape and another registered bending shapes.

High intrinsic stress on NEMS resonators based on a double clamped beam with variable cross-section can affect its first bending resonant frequency. The estimation of intrinsic stress can be included into our proposed analytic model to determine its influence on the resonant frequency of the resonators. This model can be easily used into the design phase of NEMS resonators. In addition to this, the proposed model can estimate the resonant frequency shift due to variations in the resonator's geometrical parameters. Thus, the designers could determine the resonator's adequate dimensions for a specific application that requires resonators operating between a limited frequencies range. Also through this model, the designers could study the influence of the beam's etched supports (L_1 and L_2) on its resonant frequency.

4 Conclusions

An analytical model to estimate the intrinsic stress effect on the first bending resonant frequency of NEMS resonators based on a double clamped beam with three cross-sections was developed. This model was obtained through the Rayleigh and Macaulay methods, as well as the Euler–Bernoulli beam theory. The proposed model was applied to a SiC resonator reported in the literature, which is under the influence of a tensile intrinsic stress. This resonator presented a thickness of 186 nm with total length range between 80 and 258 μm. The resonator registered a high tensile intrinsic stress close to 110 MPa, which was obtained during its fabrication process. The analytical model results were well consistent with the experimental results reported in the literature. The analytical resonant frequencies registered a relative difference less than 6.3% respect to measured frequencies. The high tensile intrinsic stress significantly increased the resonant frequency of the resonator. The proposed analytical model can be easily used in order to estimate the bending resonant frequency of this resonator type and to know the intrinsic stress influence on it.

Future research directions will include resonators subject to intrinsic stress with different structural configurations and support types. Also, the effect of a metallic layer deposited over the resonator surface must be considered in the estimation of its resonant frequency.

Acknowledgments This work was supported by the Mexican National Council for Science and Technology (CONACYT) through grants 84605 and 115976.

References

Baldwin JW, Zalalutdinov MK, Feygelson T, Pate BB, Butler JE, Houston BH (2006) Nanocrystalline diamond resonator array for RF signal processing. Diam Relat Mater 15:2061–2067. doi:10.1016/j.diamond.2006.09.009

Bokaian A (1988) Natural frequencies of beams under compressive axial loads. J Sound Vib 126:49–65. doi:10.1016/0022-460X(88)90397-5

Bolton WC (2006) Mechanical science, 3rd edn. Blackwell Publishing Ltd, Chennai

Bouwstra S, Geijselaers B (1991) On the resonant frequencies of microbridges. In: Transducers '91, international conference in solid-state sensors and actuators, San Francisco, pp 538–542

Cimalla V, Ch Foerster, Will F, Tonisch K, Brueckner K, Stephan R, Hein ME, Ambacher O (2006) Pulsed mode operation of strained microelectromechanical resonators in air. Appl Phys Lett 88:253501. doi:10.1063/1.2213950

Cimalla V, Niebelschütz F, Tonisch K, Foerster Ch, Brueckner K, Cimalla I, Friedrich T, Pezoldt J, Stephan R, Hein M, Ambacher O (2007) Nanoelectromechanical devices for sensing applications. Sens Actuators B 126:24–34. doi:10.1016/j.snb.2006.10.049

Cleland AN, Pophristic M, Ferguson I (2001) Single-crystal aluminum nitride nanomechanical resonators. Appl Phys Lett 79:2070–2072. doi:10.1063/1.1396633

Craig RR Jr (1996) Mechanics of materials, 1st edn. John Wiley & Sons Inc., New York

Ekinci KL, Roukes ML (2005) Nanoelectromechanical systems. Rev Sci Instrum 76:061101. doi:10.1063/1.1927327

Feng XL, White CJ, Hajimiri A, Roukes ML (2008) A self-sustaining ultrahigh-frequency nanoelectromechanical oscillator. Nat Nanotechnol 3:342–346. doi:10.1038/nnano.2008.125

Galef AE (1968) Bending frequencies of compressed beams. J Acoust Soc Am 44:643

Guerra DN, Imboden M, Mohanty P (2008) Electrostatically actuated silicon-based nanomechanical switch at room temperature. Appl Phys Lett 93:033515. doi:10.1063/1.2964196

Herrera-May A, Aguilera-Cortés LA, Manjarrez E, González-Palacios M (2010) Nanoelectromechanical systems: origin, applications and challenges. Interciencia 35(3):163–170 Translation of Spanish paper

Ikehara T, Zwijze RAF, Ikeda K (2001) New method for an accurate determination of residual strain in polycrystalline silicon films by analysing resonant frequencies of micromachined beams. J Micromech Microeng 11:55–60. doi:10.1088/0960-1317/11/1/309

Jackson KM, Duning J, Zorman CA, Mehregany M, Sharpe WN Jr (2005) Mechanical properties of epitaxial 3C Silicon carbide thin films. J Microelectromech Syst 14:664–672. doi:10.1109/JMEMS.2005.847933

Jun SC, Huang XMH, Manolidis M, Zorman CA, Mehregany M, Hone J (2006) Electrothermal tuning of Al–SiC nanomechanical resonator. Nanotechnology 17:1506–1511. doi:10.1088/0957-4484/17/5/057

Jun SC, Son H, Baik CW, Kim JM, Moon SW, Kim HJ, Huang XMH, Hone J (2008) Electrothermal noise analysis in frequency tuning of nanoresonators. Solid State Electron 52:1388–1393. doi:10.1016/j.sse.2008.04.033

Karabacak DM, Yakhot V, Ekinci KL (2007) High-frequency nanofluidics: an experimental study using nanomechanical resonators. Phys Rev lett 98:254505. doi:10.1103/PhysRevLett.98.254505

Karabalin RB, Feng XL, Roukes ML (2009) Parametric nanomechanical amplification at very high frequency. Nano Lett 9:3116–3123. doi:10.1021/nl901057c

Lobontiu NO (2006) Mechanical design of microresonators. McGraw Hill, New York

Lobontiu NO (2007) Dynamics of Microelectromechanical. Springer, New York

Mamin HJ, Rugar D (2001) Sub-attonewton force detection at millikelvin temperatures. Appl Phys Lett 79:3358. doi:10.1063/1.1418256

Naik AK, Hanay MS, Hiebert WK, Feng XL, Roukes ML (2009) Towards single-molecule nanomechanical mass spectrometry. Nat Nanotechnol 4:445–450. doi:10.1038/nnano.2009.152

Rao SS (2004) Mecanical Vibrations, 4th edn. Pearson Education Inc., Upper Saddle River

Stephen NG (2007) Macaulay's method for a Timoshenko beam. Int J Mech Eng Educ 35:285–292

Varshney M, Waggoner PS, Montagna RA, Craighead HG (2009) Prion protein detection in serum using micromechanical resonator array. Talanta 80:593–599. doi:10.1016/j.talanta.2009.07.032

Virgin LN (2007) Vibration of axially loaded structures. Cambridge University Press, New York

Waggoner PS, Tan CP, Bellan L, Craighead G (2009) High-Q, in plane modes of nanomechanical resonators operated in air. J Appl Phys 105:094315. doi:10.1063/1.3123767

Weaver W Jr, Timoshenko SP, Young DH (1990) Vibration Problems in Engineering, 5th edn. John Wiley & Sons Inc, New York